



HAL
open science

Understanding the NMR shifts in paramagnetic transition metal oxides using density functional theory calculations

Dany Carlier-Larregaray, Michel Ménétrier, C. P. Grey, Claude Delmas, Gerbrand Ceder

► **To cite this version:**

Dany Carlier-Larregaray, Michel Ménétrier, C. P. Grey, Claude Delmas, Gerbrand Ceder. Understanding the NMR shifts in paramagnetic transition metal oxides using density functional theory calculations. *Physical Review B: Condensed Matter and Materials Physics (1998-2015)*, 2003, 67 (17), pp.174103. 10.1103/PhysRevB.67.174103 . hal-00207928

HAL Id: hal-00207928

<https://hal.science/hal-00207928v1>

Submitted on 19 Jan 2024

HAL is a multi-disciplinary open access archive for the deposit and dissemination of scientific research documents, whether they are published or not. The documents may come from teaching and research institutions in France or abroad, or from public or private research centers.

L'archive ouverte pluridisciplinaire **HAL**, est destinée au dépôt et à la diffusion de documents scientifiques de niveau recherche, publiés ou non, émanant des établissements d'enseignement et de recherche français ou étrangers, des laboratoires publics ou privés.

Understanding the NMR shifts in paramagnetic transition metal oxides using density functional theory calculations

D. Carlier,^{1,*} M. Ménétrier,² C. P. Grey,³ C. Delmas,² and G. Ceder¹¹*Materials Science and Engineering Department, Massachusetts Institute of Technology, 77 Massachusetts Avenue, Cambridge, Massachusetts 02139*²*Institut de Chimie de la Matière Condensée de Bordeaux-CNRS and Ecole Nationale Supérieure de Chimie et Physique de Bordeaux, 87 Avenue Dr. A. Schweitzer, 33608 Pessac Cedex, France*³*Department of Chemistry, State University of New York at Stony Brook, Stony Brook, New York 11794-3400*

(Received 30 October 2002; published 8 May 2003)

The ${}^6\text{Li}$ MAS NMR spectra of lithium ions in paramagnetic host materials are extremely sensitive to number and nature of the paramagnetic cations in the Li local environments and large shifts (Fermi contact shifts) are often observed. The work presented in this paper aims to provide a rational basis for the interpretation of the ${}^6\text{Li}$ NMR shifts, as a function of the lithium local environment and electronic configuration of the transition metal ions. We focus on the layered rocksalts often found for LiMO_2 compounds and on materials that are isostructural with the K_2NiF_4 structure. In order to understand the spin-density transfer mechanism from the transition metal ion to the lithium nucleus, which gives rise to the hyperfine shifts observed by NMR, we have performed density functional theory (DFT) calculations in the generalized gradient approximation. For each compound, we calculate the spin densities values on the transition metal, oxygen and lithium ions and map the spin density in the $M\text{-O-Li}$ plane. Predictions of the calculations are in good agreement with several experimental results. We show that DFT calculations are a useful tool with which to interpret the observed paramagnetic shifts in layered oxides and to understand the major spin-density transfer processes. This information should help us to predict the magnitudes and signs of the Li hyperfine shifts for different Li local environments and t_{2g} vs e_g electrons in other compounds.

DOI: 10.1103/PhysRevB.67.174103

PACS number(s): 76.20.+q, 61.50.Ah

I. INTRODUCTION

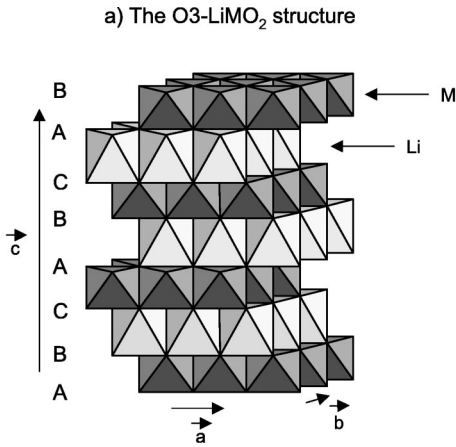
The number of NMR studies of Li-intercalation oxides has increased dramatically over the last few years and systems with an increasingly large number of transition metal ions, doping elements, oxidation states, and structural types have now been investigated with ${}^6\text{Li}$ and ${}^7\text{Li}$ NMR.^{1–10} The lithium MAS NMR spectra are sensitive to the presence of paramagnetic cations in the local coordination environment of the lithium ions. These paramagnetic ions create spin density at the lithium nucleus, which can lead to large hyperfine shifts in the NMR [and electron spin resonance (ESR)] spectra, providing information concerning the lithium local environment. For many systems, several resonances with large positive or negative hyperfine shifts have been observed, and their assignments are not always obvious. In this paper, we show by means of density functional theory (DFT) calculations that a rational interpretation of the shifts in terms of the electronic configuration and geometric environment of the transition metal and Li ions can be provided. We also analyze the spin-density transfer mechanisms from the transition metal ion to the lithium nucleus. Application of this method to other systems may result in an increased level of confidence with which shifts are assigned, and may increase the level of information that can be obtained from the NMR spectra of paramagnetic oxides.

Fermi contact NMR shifts have been calculated *ab initio* in molecular solids within the unrestricted Hartree Fock method and with DFT,^{11–14} however, no such studies, to our knowledge, have been performed in transition metal oxides

or other materials with a large number of electrons. The Fermi contact interaction (i.e., the hyperfine interaction) can also be observed by ESR, and *ab initio* calculations of this interaction have been performed on small systems and compared with experimental ESR results.¹⁵

Here we focus on two types of layered compounds: La_4LiMO_8 ($M=\text{Cr, Mn, Ni}$) isostructural to K_2NiF_4 and LiMO_2 ($M=\text{Co, Cr, Mn, Fe, Ni}$) and substituted $\text{LiM}_y\text{Co}_{1-y}\text{O}_2$ ($M=\text{Cr, Ni}$) isostructural to $\alpha\text{-NaFeO}_2$ or NaNiO_2 depending on the transition metal ion. The LiMO_2 ($M=\text{Co, Cr, Mn, Fe, Ni}$) phases are of particular interest as positive electrode materials for lithium-ion batteries. LiCoO_2 has been used since 1994 in commercial lithium batteries. Nickel substitution for cobalt plays an important role for increasing the capacity, and the substituted $\text{Li}_x\text{Ni}_y\text{Co}_{1-y}\text{O}_2$ systems have been extensively studied over the past few years.^{16–24} More recently, materials such as $\text{Li}[\text{Co}_x\text{Li}_{(1-x)/3}\text{Mn}_{(2-2x)/3}\text{O}_2]$,^{25–27} $\text{Li}[\text{Cr}_x\text{Li}_{(1-x)/3}\text{Mn}_{(2-2x)/3}\text{O}_2]$,^{10,28} and $\text{Li}[\text{Ni}_x\text{Li}_{(1-2x)/3}\text{Mn}_{(2-x)/3}\text{O}_2]$ ^{29–31} have also been proposed as good candidates to replace LiCoO_2 . The interpretation of the ${}^6\text{Li}$ NMR spectra of these substituted systems is not always obvious as several lithium crystallographic sites and paramagnetic environments may exist.

The LiMO_2 phases adopt a layered “O3” structure,³² built from alternate sheets of edge-sharing MO_6 and LiO_6 octahedra (Fig. 1). The trivalent nickel and cobalt ions in these materials exhibit a low spin state,^{20,33} while the trivalent manganese and iron are in a high spin state.^{34,35} Thus the electronic configurations are Cr^{3+} ($t_{2g}^3 e_g^0$), Mn^{3+} ($t_{2g}^3 e_g^1$),



b) The different types of interactions in the O3-LiM_yCo_{1-y}O₂ structure

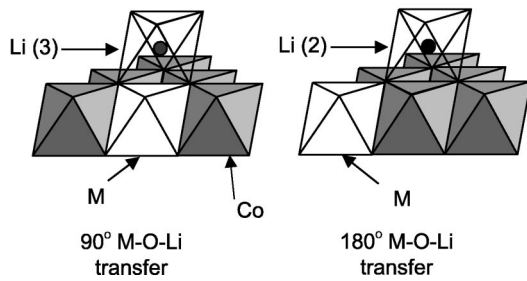


FIG. 1. Structure of the O3-LiMO₂ and the LiM_yCo_{1-y}O₂ phases (a) with the different types of interactions (90° and 180°) (b). The same notation for the Li(2) and Li(3) sites is used throughout this paper for the LiM_yCo_{1-y}O₂ phases (see Table III).

Fe³⁺ ($t_{2g}^3 e_g^2$), Co³⁺ ($t_{2g}^6 e_g^0$), Ni³⁺ ($t_{2g}^6 e_g^1$). The LiCrO₂, LiFeO₂, LiCoO₂ cells are all rhombohedral ($R-3m$). The Ni³⁺ and Mn³⁺ ions can exhibit a Jahn-Teller distortion, leading to a monoclinic distortion (space group $C2/m$) of the unit cells. However, a macroscopic distortion has only been observed for LiMnO₂.^{36,37} In LiNiO₂, a local distortion was seen by x-ray absorption analysis,³⁸ but on average the structure remains rhombohedral. The lithium ions in LiMO₂ compounds with the $R-3m$ or $C2/m$ structure can interact with transition metal ions as first or second neighbors (Fig. 1). These two interactions are termed the 90° and 180° ($M-O-Li$) interactions, respectively, because of the angle of the $M-O-Li$ bond.

In order to also consider $M-O-Li$ interactions with different geometries, we chose to study the La₄LiMO₈ ($M = Cr, Mn, Ni$) phases, which are isostructural to K₂NiF₄.³⁹⁻⁴¹ To our knowledge, only the La₄LiMnO₈ (Mn³⁺) and La₄LiNiO₈ (Ni³⁺) materials have been synthesized, but as Cr³⁺ is isoelectronic to Mn⁴⁺, and as the Mn⁴⁺-containing material La₃SrLiMnO₈ has been synthesized,⁴⁰ we also studied the hypothetical La₄LiCrO₈ material by first principles calculations. The charge difference between the Li and Ni or Mn ions leads to a strong ordering interaction, and hence, the La₄LiMO₈ ($M = Ni, Mn$) phases exhibit a chessboard-type Li/M ordering in the xy plane, leading to a $\sqrt{2} \times \sqrt{2} \times 1$ supercell of the original K₂NiF₄ tetragonal unit cell (Fig. 2).³⁹⁻⁴¹ The symmetry of these phases is then A-centered

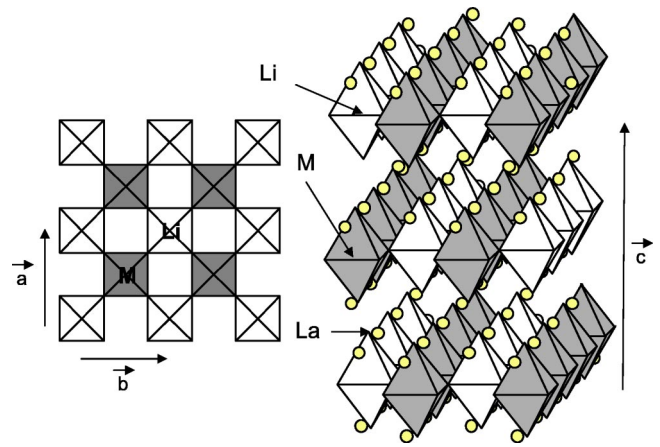


FIG. 2. Structure of the ordered La₄LiMO₈ phases. The (xy) plane Li/M ordering is shown on the left.

orthorhombic ($Ammm$). This symmetry lowering was observed by x-ray diffraction for La₄LiNiO₈ (Ref.³⁹) and La₃SrLiMnO₈ in one study,⁴⁰ but not for La₄LiMnO₈. Very recently, Burley *et al.* showed by electron diffraction and NMR that both La₃SrLiMnO₈ and La₄LiMnO₈ exhibit cation ordering in the perovskitelike sheets of the K₂NiF₄ structure, but that the stacking of the sheets is disordered along [001] in both these compounds.⁴¹ The lithium first coordination sphere is identical in the ordered and disordered structures, the lithium ion interacting through 180° oxygen bonds with four transition metal ions (Fig. 2). The transition metals are in a distorted tetragonal environment in this material, allowing the effect of lifting the degeneracy of the e_g orbitals on the electron spin densities to be explored in the calculations.

In this paper, we present DFT calculations of the spin density around the transition metal, the oxygen and the lithium ions, and use this information to predict the magnitudes and signs of the Li hyperfine shifts as a function of the electronic structure of the surrounding transition metals. A brief introduction to the NMR theory and to the relevant DFT methodology is presented in the following two sections (Secs. II and III, respectively) before comparing the experimental (NMR) results and the DFT calculations in Secs. IV and V.

II. NMR CONTACT SHIFTS

The NMR shift ($\Delta\omega/\omega_0$) induced by the Fermi contact interaction in materials with 3d metal ions is proportional to the electron spin (i.e., unpaired electron) density at the nucleus $\rho(r=0)$. This quantity depends itself on the Fermi constant A_c and on the time-averaged value of the electron spin in the material $\langle S_z \rangle$:^{42,43}

$$\frac{\Delta\omega}{\omega_0} = -\frac{A_c}{\omega_0 \hbar} \langle S_z \rangle. \quad (1)$$

A_c indicates how much of the spin density is at the site of the nucleus of interest and governs the direction of the shift. $\langle S_z \rangle$ is proportional to the magnetic molar susceptibility χ_M (m³/mol) and can be expressed by⁴⁴

$$\langle S_z \rangle = - \frac{B_0}{\mu_0 g N_0 \mu_B} \chi_M, \quad (2)$$

where μ_0 denotes the permeability, g is the electron g factor, μ_B is the Bohr magneton, N_0 is Avogadro's number, and B_0 is the external applied field. Typically, only the time-averaged value of S_z , $\langle S_z \rangle$, is meaningful with respect to the NMR experiment (at ambient temperatures) since the electrons (in systems that can be studied by NMR) relax several orders of magnitude faster than the coupling frequency A_c/h (Hz). In transition metal oxides, the Fermi contact shift is generally considered to be additive, so that the shift due to many magnetic ions may be obtained from a sum of the shifts induced by each magnetic ion.

The approach outlined above is only strictly valid for systems where the orbital angular moment is quenched and the "spin-only" expressions may be used to calculate the magnetic moments. This is, however, a reasonable approximation for many transition metal ions.

III. FIRST PRINCIPLES CALCULATIONS

The NMR contact shift will have the same sign and will be proportional to the spin density at the nucleus arising from spin polarized transition metal ions. Scalar spin-polarized DFT is used in this paper to calculate the electron spin density at position R , by calculating the difference between the electron density of the majority spin and that of the minority spin

$$\rho(R) = \sum_i^{occ} [|\Psi_{i\uparrow}(R)|^2 - |\Psi_{i\downarrow}(R)|^2], \quad (3)$$

where $\Psi_{i\uparrow}$ and $\Psi_{i\downarrow}$ are the Kohn-Sham orbitals for the majority and minority spins, respectively. By convention, we will assign the term "up spin" to the majority spin on the transition metal ion, which will, hence, align parallel to the applied magnetic field in an NMR experiment.

First principles calculations were performed using DFT in the generalized gradient approximation (GGA) with the pseudopotential method as implemented in the Vienna *ab initio* Simulation Package (VASP).⁴⁵ Such a method, as opposed to all electrons calculations allows one to treat large supercells, as required for the La_4LiMO_8 and substituted LiMO_2 phases. A plane wave basis set with a cutoff energy of 400 eV was chosen. The reciprocal space sampling was performed with a k -point grid of $10 \times 10 \times 10$ for the rhombohedral LiMO_2 and $10 \times 10 \times 6$ for the monoclinic LiMO_2 structure. Grids of $3 \times 3 \times 2$ and $6 \times 6 \times 6$ size were, respectively, sampled in the Brillouin zones of the $\text{LiM}_{1/8}\text{Co}_{7/8}\text{O}_2$ and La_4LiMO_8 structures. All structures are relaxed and the final energies of the optimized geometries were recalculated so as to correct for the changes in basis during relaxation. In principle, the contact interaction depends only on the electronic spin density at the nucleus, but here, since we use a pseudopotential method, this quantity is not accurate enough and it is preferable to track the change of the spin density in the vicinity of the nucleus, as done in the following.

TABLE I. Experimental shifts observed in several layered oxides. For the $\text{LiM}_y\text{Co}_{1-y}\text{O}_2$ compounds, only the major peaks are given. All shifts are referenced to a 1 M LiCl solution.

	Observed shifts (ppm)	Ref.
<hr/>		
O3-LiMO ₂		
LiCrO ₂	17	10
LiMnO ₂	143	47
LiFeO ₂	1000	54
LiCoO ₂	0	48–53
Li _{0.98} Ni _{1.02} O ₂	726	54
LiM _y Co _{1-y} O ₂		
<hr/>		
LiCr _{0.10} Co _{0.90} O ₂	35	10
	0	
	-70	
LiNi _{0.30} Co _{0.70} O ₂	110	1
	0	
	-15	
<hr/>		
La ₄ LiMO ₈		
La ₄ LiNiO ₈	100	55
La ₄ LiMnO ₈	-491	41
La ₃ SrLiMnO ₈	-500	41
<hr/>		

The partial density of state (DOS) plots are obtained by projecting the wave functions in a sphere around each ion (using the ionic radius of each element as found in Shannon and Prewitt's table⁴⁶) and onto the five types of $3d$ orbitals. To evaluate the spin on the lithium nucleus, the spin density was integrated in a sphere around Li. This method will not provide a quantitative estimation of the contact shift, but will allow the sign and the relative sizes of different shifts to be determined. Methods for obtaining quantitative values of the shift will be discussed in Sec. V C.

Since the compounds considered here are paramagnetic at room temperature, in our calculations, the spins of the paramagnetic transition metal ions are assumed to be aligned with the applied magnetic field, however, no assumption is made regarding the resultant spin density around the lithium ions, which is an output of the calculation. We also discuss possible local antiferromagnetic couplings between transition metal ions, that can influence the resulting spin transfer on Li.

IV. RESULTS

A. Summary of experimental shift data

Table I summarizes the experimental shifts observed for several layered oxides. Only the major resonances observed for the $\text{LiM}_y\text{Co}_{1-y}\text{O}_2$ compounds are given and their assignments will be discussed later. The shifts are all referenced to a 1 M LiCl solution. The LiCoO_2 compound is diamagnetic, because of the electronic configuration of the Co^{3+} ions. It, therefore, does not exhibit a contact shift, in contrast to all the other LiMO_2 compounds, which all exhibit positive shifts. Note that the shift in LiFeO_2 could not be precisely determined, because of the large line broadening present for

TABLE II. The relaxed cell parameters and bonds lengths from first principles calculation of the LiMO_2 and La_4LiMO_8 phases. The experimental values (when available) are given in parenthesis.

	SG	a (Å)	b (Å)	c (Å)	β (°)	d_{M-O} (Å)	d_{Li-O} (Å)
$\text{La}_4\text{LiCrO}_8$	$Ammm$	5.42		13.77		1.93×4 2.11×2	1.90×4 2.31×2
$\text{La}_4\text{LiMnO}_8$	$Ammm$	5.35 (5.36)		13.05 (12.96)		1.88×4 2.36×2 (1.89×4) (2.32×2)	1.90×4 2.37×2 (1.89×4) (2.32×2)
$\text{La}_4\text{LiNiO}_8$	$Ammm$	5.31 (5.3)		12.94 (12.85)		1.86×4 2.28×2 (1.87×4) (2.18×2)	1.90×4 2.32×2 (1.91×4) (2.30×2)
LiCrO_2	$R-3m$	2.9 (2.9)		13.87 (14.41)		2	2.07
LiMnO_2	$R-3m$	2.92		14.03		2.02	2.08
LiMnO_2	$C2/m$	5.36 (5.45)	2.81 (2.81)	5.23 (5.4)	112.73 (116.07)	1.93×4 2.31×2 (1.98×4) (2.40×2)	2.04×4 2.18×2 (2.16×4) (1.44×2)
LiFeO_2	$R-3m$	2.9293 (2.95)		14.2289 (14.57)		2.05	2.09
LiCoO_2	$R-3m$	2.83 (2.82)		13.58 (14.05)		1.93 (1.92)	2.05 (2.09)
LiNiO_2	$R-3m$	2.85 (2.87)		13.72 (14.19)		1.96 (1.93)	2.05 (2.15)
LiNiO_2	$C2/m$	5.12	2.78	5	110.18	1.91×4 2.11×2	2.03×4 2.11×2
$\text{LiCr}_{1/8}\text{Co}_{7/8}\text{O}_2$	$P2/m$	4.9	5.66	9.23	79.95	$d_{Cr-O} = 1.98$ $d_{Co-O} = 1.94$	~ 2.05
$\text{LiNi}_{1/8}\text{Co}_{7/8}\text{O}_2$	$P2/m$	4.89	5.65	9.18	79.86	$d_{Ni-O} = 1.97 \times 4$ 1.98×2 $d_{Co-O} \sim 1.93$	~ 2.05

this sample, probably due to large dipolar interactions. However, the isotropic shift was estimated to be approximately 1000 ppm.⁵⁴ Several resonances are observed for the $\text{LiM}_y\text{Co}_{1-y}\text{O}_2$ substituted phases, which are positively or negatively shifted depending on the lithium local environment.^{1,10} The La_4LiMO_8 phases studied show either positive or negative shifts depending on the transition metal ion.^{41,55}

B. Calculations

The relaxed cell parameters and bondlengths obtained from our first principles calculation are given in Table II and are compared to the experimental values when available. The calculations agree well with experiments: in all cases, the bondlengths are predicted to within 2% of experiment. For

each compound we also checked that the electronic configuration obtained for the transition metal ion was consistent with the experimentally observed electronic states.

For LiNiO_2 and LiMnO_2 , two different structures were considered: the rhombohedral (MO_6 not Jahn-Teller distorted) and the monoclinic (MO_6 Jahn-Teller distorted). As already reported, the monoclinic structure is predicted from first principles calculation to be the more stable one by -248 meV for LiMnO_2 (Ref.⁵⁶) and by only -11 meV for LiNiO_2 .⁵⁷ These values are consistent with the observations of a strong cooperative distortion in LiMnO_2 and a noncooperative one in LiNiO_2 at room temperature.³⁶⁻³⁸

Figure 3 shows the total electron-spin difference, as a function of the integration radius around Li for the La_4LiMO_8 (a), LiMO_2 (b), and $\text{LiM}_y\text{Co}_{1-y}\text{O}_2$ [(c) and (d)]

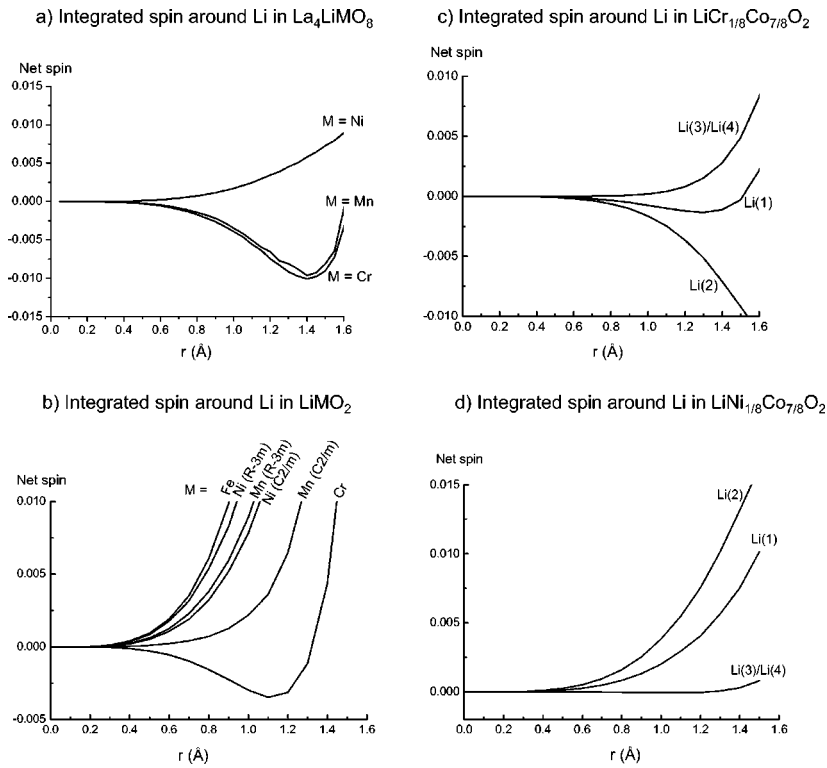


FIG. 3. The total electron-spin difference, defined by the difference between the majority minus minority electron spin density, as a function of the integration radius around Li in the La_4LiMO_8 (a), the LiMO_2 (b), and the $\text{LiM}_y\text{Co}_{1-y}\text{O}_2$ (c) and (d) phases.

phases. As the shortest Li-O bond is observed in the La_4LiMO_8 phases (1.90 Å; Table II), integration beyond a radius of 1 Å includes density that should more likely be assigned to the oxygen ions. This is clearly seen for the $\text{La}_4\text{LiMnO}_8$ and $\text{La}_4\text{LiCrO}_8$ compounds [Fig. 3(a)], where the spin density changes sign for $r > 1.4$ Å. We therefore integrate the spin in a 0.8 Å radius sphere [the ionic radius for a lithium ion in an octahedral site is 0.76 Å (Ref.⁴⁶). Figure 4(b) compares these values to the experimental shifts, already given in Table I.

The La_4LiMO_8 phases ($M = \text{Cr}, \text{Mn}, \text{Ni}$). A large and positive spin density is observed near the lithium nucleus in $\text{La}_4\text{LiNiO}_8$ whereas a negative spin density is observed for both $\text{La}_4\text{LiMnO}_8$ and $\text{La}_4\text{LiCrO}_8$ [Fig. 3(a)]. Therefore according to Eqs. (1), (2), and (3), the signal recorded by NMR for lithium in these materials is predicted to be positive for $\text{La}_4\text{LiNiO}_8$ and negative for $\text{La}_4\text{LiMnO}_8$. As Cr^{3+} is isoelectronic to Mn^{4+} , a negative shift for the Mn^{4+} compound $\text{La}_3\text{SrMnO}_8$ is also predicted. These results are in good agreement with the experimental data. The calculations also reproduce the fact that the absolute value of the shift for $\text{La}_4\text{LiMnO}_8$ is larger than the one for $\text{La}_4\text{LiNiO}_8$ (Fig. 4).

The LiMO_2 phases. Positive spin densities are observed for all the different paramagnetic LiMO_2 phases ($M = \text{Cr}, \text{Mn}, \text{Fe}, \text{Ni}$) except LiCrO_2 [Fig. 3(b)], and are therefore in good agreement with the experimental shifts except for LiCrO_2 , where the measured shift is small and positive (Fig. 4). The difference between the monoclinic and rhombohedral LiNiO_2 and LiMnO_2 also indicates that the Jahn-Teller distortion reduces the spin density on Li. These points will be discussed below.

The $\text{LiM}_y\text{Co}_{1-y}\text{O}_2$ phases. Some $\text{LiM}_y\text{Co}_{1-y}\text{O}_2$ phases, where M^{3+} is a paramagnetic ion, have been studied experi-

mentally. As Co^{3+} remains diamagnetic in these samples, one can differentiate between the lithium local environments by^{6,7} Li NMR in terms of the number of first and second neighbors M^{3+} ions. Several signals are thus recorded, but their assignment in terms of the arrangements of the paramagnetic ions surrounding the Li is not always obvious. Marchal *et al.* assigned the resonance at +110 and -15 ppm (Table I) in $\text{LiNi}_y\text{Co}_{1-y}\text{O}_2$ to the lithium ions interacting with Ni^{3+} as first and second neighbors,¹ respectively. Lee *et al.* assigned the +35 and -70 ppm (Table I) resonances in $\text{LiCr}_y\text{Co}_{1-y}\text{O}_2$ to the lithium ions interacting with Cr^{3+} as first and second neighbors, respectively.¹⁰ Resonances close to 0 ppm are unambiguously assigned in both samples to the lithium ions that are surrounded only by diamagnetic Co^{3+} ions as first and second neighbors.^{1,10} The signals assignments were based on the application of the Goodenough and Kanamori superexchange rules to the M -O-Li interactions.⁵⁸ These rules are usually applied to determine the type of magnetic coupling (ferromagnetic or antiferromagnetic) between magnetic ions,⁵⁸ but extended to the M -O-Li systems, in order to determine the sign and the magnitude of the contact shift.

In order to determine how the spin density on the lithium nucleus depends on its paramagnetic environment we consider a supercell of the primitive LiCoO_2 cell with the $\text{LiM}_{1/8}\text{Co}_{7/8}\text{O}_2$ ($M = \text{Cr}, \text{Ni}$) composition. The M^{3+} ions are arranged so as to give alternating layers of $(M_{1/4}\text{Co}_{3/4})$ and pure CoO_2 layers along the z direction. The cell was designed so as to have several different lithium environments with respect to the number and arrangements of M^{3+} ions (Table III). The notation used to describe the different M -O-Li interactions is identical to that used in Fig. 1(b). The results given in Fig. 4(b) correspond to single 90° and 180°

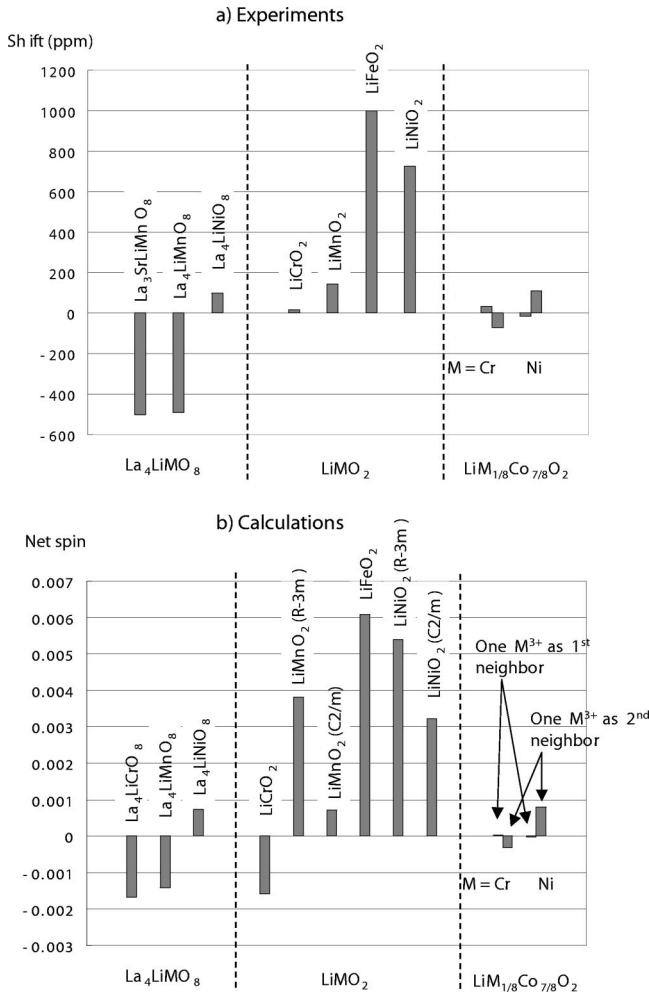


FIG. 4. Experimental shifts (from Table I) (a), compared with the values of the net spin integrated in a 0.8 \AA sphere for all the materials considered (b). Results for single 90° and 180° M^{3+} -O-Li interactions are shown for the $\text{LiM}_{1/8}\text{Co}_{7/8}\text{O}_2$ phases.

M -O-Li interactions, i.e., the spin density calculated for Li(2) has been divided by 2. The spin density calculated for Li(1) corresponds to approximately the sum of the spin densities calculated for Li(2) and Li(3) (i.e., one 90° M -O-Li interaction + one 180° M -O-Li interaction), indicating that the shifts caused by two M ions are additive.

The calculations presented in Fig. 4 are in good agreement with the signal assignment made for $\text{LiCr}_{0.10}\text{Co}_{0.90}\text{O}_2$, as a negative spin density is obtained for Li interacting with Cr^{3+} as a second neighbor (a 180° M -O-Li interaction), i.e. half the spin density calculated for the Li(2) site, whereas

TABLE III. The different lithium environment in the $\text{LiM}_{1/8}\text{Co}_{7/8}\text{O}_2$ supercell considered in the calculations.

	M^{3+} as 1st neighbor 90° interaction	M^{3+} as 2nd neighbor 180° interaction
Li(1)	1	1
Li(2)	0	2
Li(3)/Li(4)	1	0

weaker and positive spin density is obtained for Li(3) which has only one M -O-Li 90° interaction. However, for $\text{LiNi}_{0.30}\text{Co}_{0.70}\text{O}_2$, calculations predict that a 180° interaction leads to a large, positive shift and that a 90° interaction leads to a small, negative shift, which is the opposite of the assignment reported previously.

V. DISCUSSION

A. NMR shift mechanisms

In order to understand the origin of the contact shifts and to be able to predict shifts in other compounds, we attempt below to rationalize the spin transfer mechanisms by suggesting general rules, which will then be discussed for each specific case. In the following, the $3d$ atomic orbitals of the transition metal ion M will be referred to as t_{2g} and e_g for an ideal and as d_{xy} , d_{xz} , d_{yz} , d_{z^2} , and $d_{x^2-y^2}$ for a distorted octahedral site. The valence orbitals of the oxygen ion will be referred to as p_σ and p_π depending on the type of overlap of the $2p$ orbitals with the M $3d$ orbitals. The Li valence atomic orbital will be referred to as $2s$ (or s). Overlap of the M e_g , O $2p$, and Li $2s$ orbitals leads to a bonding orbital with a large contribution from the oxygen orbital, which we shall refer to as the e_g - p_σ - s orbital and to an antibonding orbital with a large M contribution referred to as the e_g^* - p_σ - s orbital. In a first approximation, the M t_{2g} orbitals can be considered to be nonbonding, however, we will clearly see that in some cases, the contact shift observed for Li cannot be explained without considering a mixing between the M t_{2g} and Li s orbitals. In the materials studied here, the O p_π orbital is also involved in this mixing, but one has to notice that this orbital is not necessary for this transfer. Spin transfer between two sites results essentially from the sum of two contributions with opposite signs.

Spin delocalization (or hybridization). Li, O, and M orbitals with the correct symmetry can overlap to form a spin orbital in the crystal. Therefore, a given spin polarization is maintained along the M -O-Li path and the spin transfer from M to Li is positive (i.e., aligned with the external magnetic field). This mechanism is illustrated in Fig. 5(a) for 90° and 180° M -O-Li interactions.

Spin polarization. Due to the exchange interaction, the unpaired electrons in the M orbitals polarize the other doubly occupied crystalline orbitals. This mechanism is illustrated in Fig. 5(b) in the case of a 90° and 180° M -O-Li interactions, where the t_{2g} - p_π - s and the bonding e_g - p_σ - s crystalline orbitals are, respectively, polarized by other unpaired electrons located on M . Because of the exchange interaction, an electron with the same spin as the transition metal unpaired electron spends more time near M than an electron with the opposite spin (actually, two nonequivalent spin orbitals are involved). Therefore positive spin density at the transition metal is increased while negative spin density is induced on the p - s oxygen and lithium orbitals. Such a mechanism leads to a negative spin transfer from M to Li.

The mechanisms described above are similar to the one described in Ref. ¹⁴ for spin transfer from the transition metal ion to the oxygen ions in molecules and molecular solids.

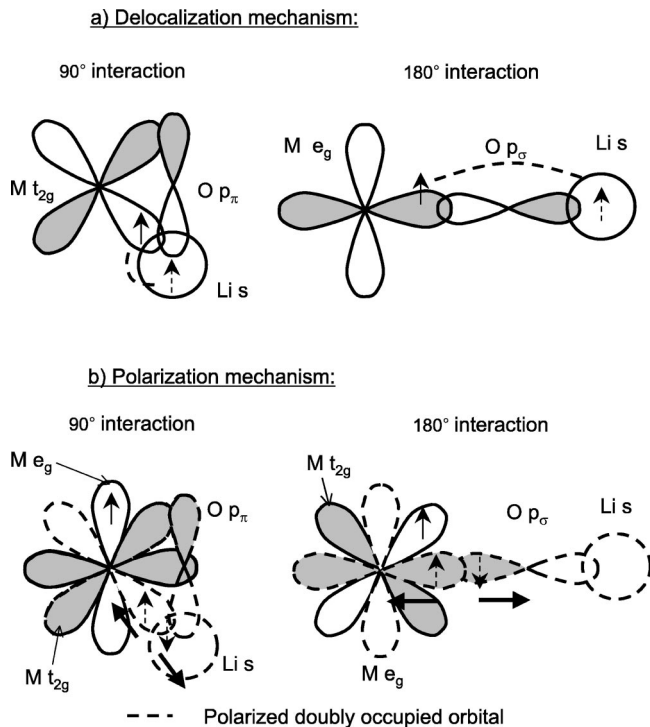


FIG. 5. The different M -O-Li spin transfer mechanisms: (a) the delocalization mechanism, (b) the polarization mechanism. See text.

The total spin transfer from a transition metal ion to the Li site is the sum of the spin transferred by delocalization and polarization from each transition metal ion. The interaction geometry of the specific system needs to be considered, in order to determine the dominant mechanism, but in general, the shift caused by the delocalization mechanism is larger than that for the polarization mechanism. Jahn-Teller distortions of the MO_6 octahedra also have to be treated separately as they affect the type of e_g orbital (d_{z^2} vs $d_{x^2-y^2}$) involved in the transfer mechanism. These points will be discussed further.

B. Discussion for specific materials

The La_4LiMO_8 ($M=Cr, Mn, Ni$) phases. The La_4LiMO_8 ($M=Cr, Mn, Ni$) phases exhibit only 180° M -O-Li interactions. In these compounds the LiO_6 and MO_6 octahedra are elongated along the z direction (Fig. 2 and Table II), so that the degeneracy of the t_{2g} and e_g orbitals is lifted. For the e_g orbitals, the d_{z^2} orbital is stabilized whereas the $d_{x^2-y^2}$ one is destabilized with respect to a regular MO_6 octahedra with intermediate M -O bondlengths. The effect of the tetragonal field on the t_{2g} orbitals is weaker, but also leads to a lifting of the degeneracy, resulting in nondegenerate d_{xz} and d_{yz} and d_{xy} orbitals. A similar effect is observed following a Jahn-Teller distortion of a MO_6 octahedron.

The calculated spin polarization density map in the (xy) plane for the La_4LiMO_8 ($M=Cr, Mn, Ni$) compounds is plotted in Fig. 6. Table IV shows the different mechanisms that occur in these systems.

In La_4LiCrO_8 , the Cr^{3+} ions have a $d_{xy}^1 d_{xz}^1 d_{yz}^1$ electronic state as seen on the DOS (Fig. 7). The single spin located in

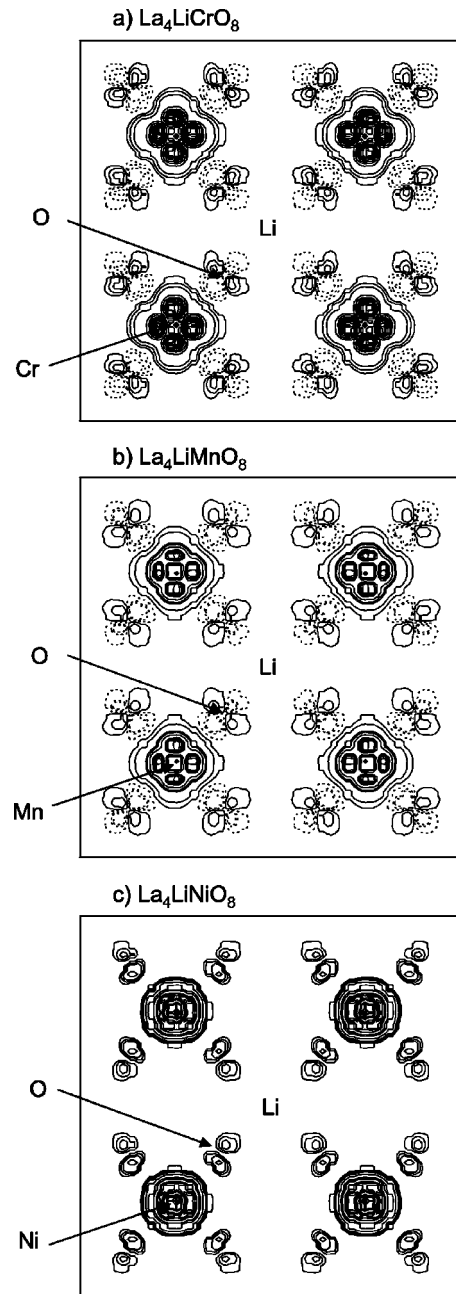
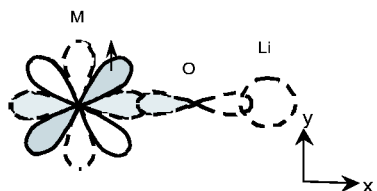
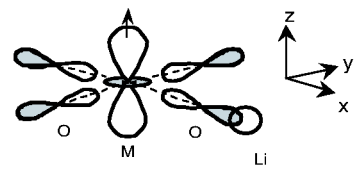
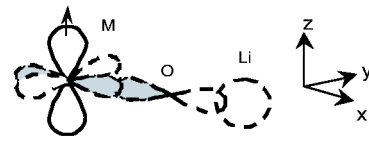
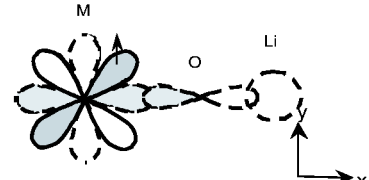
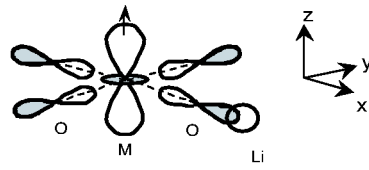
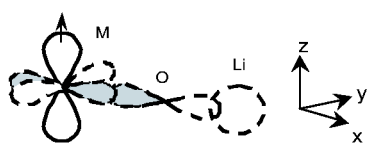


FIG. 6. Calculated spin polarization density map in the (xy) plane in La_4LiMO_8 structure for $M=Cr$ (a), $M=Mn$ (b), and $M=Ni$ (c) from DFT calculations: solid line and dashed contours indicate positive and negative spin densities, respectively. Different contour steps were taken around O and M since the spin difference is much larger on M . The position of each ion is also indicated.

the d_{xy} orbital is clearly seen in Fig. 6(a), as the single electron in the (xy) plane is located in an orbital that points between the oxygen ions. No delocalization from the Cr^{3+} to the Li is possible therefore the spin transfer occurs through the polarization mechanism. The d_{xy} , d_{xz} , and d_{yz} electron spins polarize the electrons in the bonding $d_{x^2-y^2}-p_{\sigma}-s$ orbital leading to a positive spin near the transition metal and to a negative one on the O p_{σ} orbital that points towards Cr^{3+} and Li. The polarization of the $d_{x^2-y^2}-p_{\sigma}$ orbital is also

TABLE IV. Illustration of the different mechanisms that result in transfer of spin density from a transition metal ion M to Li in the layered La_4LiMO_8 ($M = \text{Cr}, \text{Mn}, \text{Ni}$) materials.

M in La_4LiMO_8	involved spin orbital	geometry	M-O-Li transfer	resulting sign on Li
Cr^{3+} (d^3)	d_{xy}, d_{xz}, d_{yz}	180°	polarization of the $d_{x^2-y^2}$ - p_σ -s orbital 	negative
Mn^{3+} (d^4)	d_{z^2}	180°	delocalization (d_{z^2} - p_σ -s hybridization) 	positive
			polarization of the $d_{x^2-y^2}$ - p_σ -s orbital 	negative
	d_{xy}, d_{xz}, d_{yz}	180°	polarization of the $d_{x^2-y^2}$ - p_σ -s orbital 	negative
Ni^{3+} (d^7)	d_{z^2}	180°	delocalization (d_{z^2} - p_σ -s hybridization) 	positive
			polarization of the $d_{x^2-y^2}$ - p_σ -s orbital 	negative

seen in the partial DOS plotted for Cr^{3+} in the $-6 \text{ eV} < E < -3 \text{ eV}$ region (Fig. 7): more up-spin $d_{x^2-y^2}$ states are occupied than down spin ones. As a result, the NMR shift is predicted to be negative. Notice also that a positive spin

density is obtained for the O p_π orbital that forms a π bond with the d_{xy} orbital [Fig. 6(a)] because of the delocalization mechanism. These orbitals, however, do not have a net overlap with the Li $2s$ orbital but can participate to the transfer

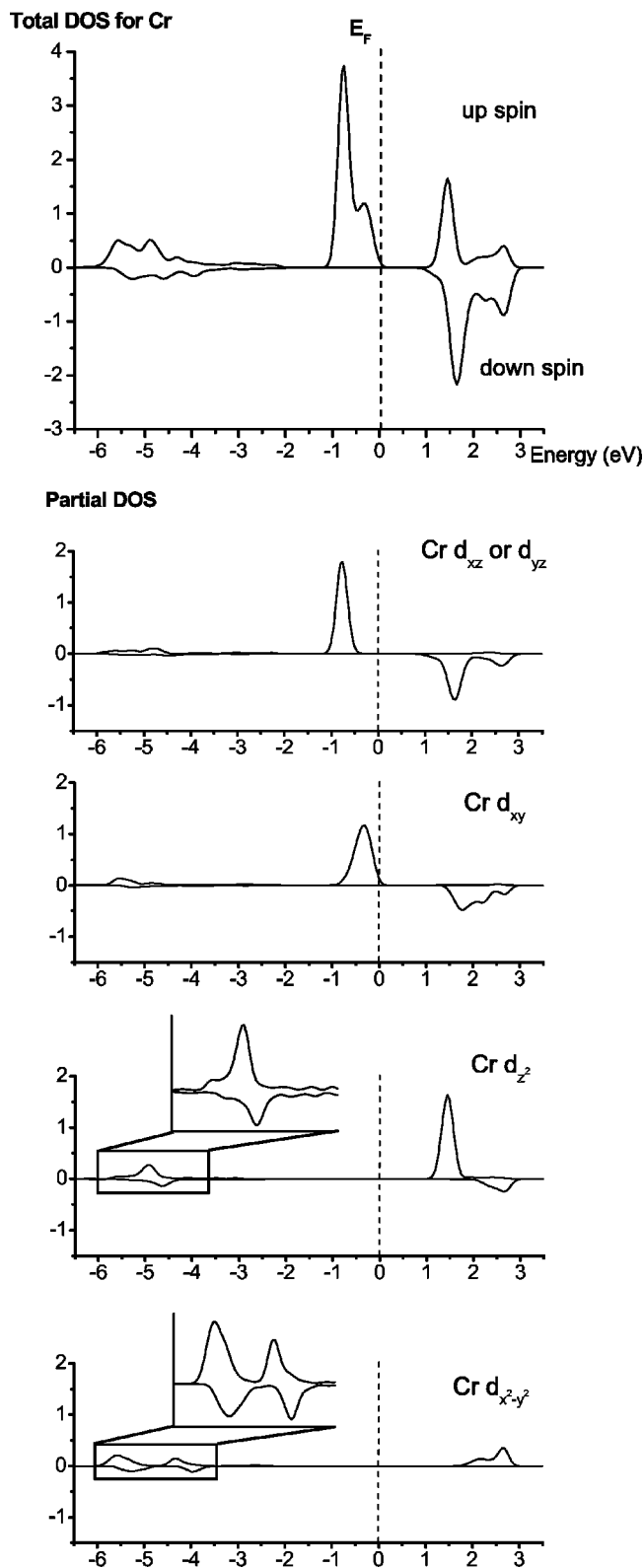


FIG. 7. The calculated total and partial density of state on Cr in $\text{La}_4\text{LiCrO}_8$.

via a polarization mechanism occurring on O: the p_π orbital polarizes the p_σ orbital that overlaps with Li 2s. Such a transfer would result in a negative spin transfer on Li, but should be small compared to the others. Therefore, to a first

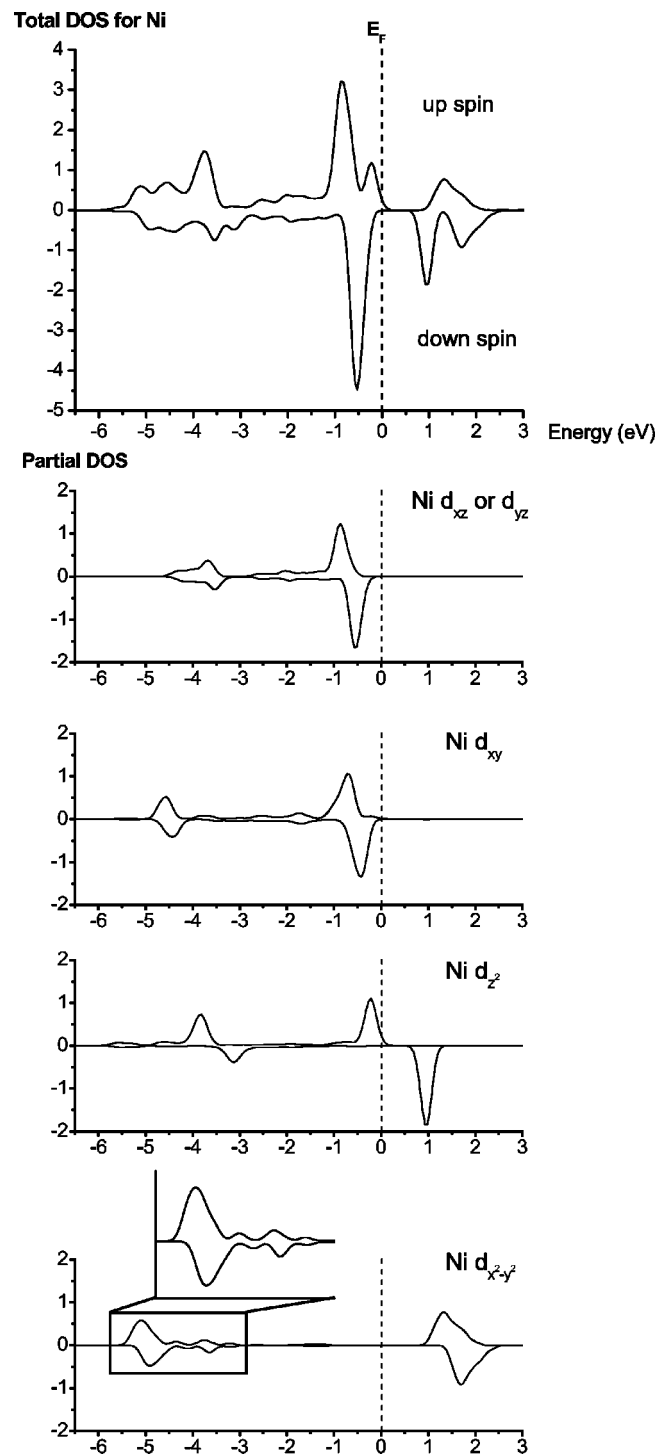


FIG. 8. The calculated total and partial density of state on Ni in $\text{La}_4\text{LiNiO}_8$.

approximation this mechanism does not contribute to the Li hyperfine shift.

In $\text{La}_4\text{LiNiO}_8$, the Ni^{3+} ion is low spin with an unpaired electron located in the d_{z^2} orbital as seen in the calculated DOS (Fig. 8). Note that a gap exists between the d_{z^2} and the $d_{x^2-y^2}$ spin up orbitals due to the tetragonal symmetry. The energy difference between the peak density of states for the d_{z^2} and the $d_{x^2-y^2}$ spin up orbitals is about 1.7 eV in

$\text{La}_4\text{LiNiO}_8$ whereas it is only 0.2 eV in monoclinic LiNiO_2 .⁵⁷ Two mechanisms with opposite spin transfer occur for the $180^\circ \text{Ni}^{3+}\text{-O-Li}$ interaction (Table IV): a delocalization mechanism involving the $\text{Ni}^{3+}d_{z^2}$, O p_σ , and Li $2s$ orbitals, leading to a positive spin on Li and a polarization of the bonding $d_{x^2-y^2}\text{-}p_\sigma\text{-}s$ orbital by the d_{z^2} unpaired electron, as seen in the Ni^{3+} partial DOS (Fig. 8), although clearly weaker than for the Cr^{3+} case (Fig. 7). Some positive spin density is located in the $d_{x^2-y^2}$ orbital lobes that point towards the oxygen ions [Fig. 6(c)]. This mechanism leads to negative spin in the Li s orbital.

The calculated map in the (xy) plane of the spin polarization density for this compound is given in Fig. 6(c). Since the spin density on Li, i.e., the resulting NMR shift due to Ni^{3+} is predicted to be positive [Figs. 3 and 6(c)], the polarization effect is weaker than the delocalization one in this case.

In $\text{La}_4\text{LiMnO}_8$, the Mn^{3+} ion exhibits a high-spin $d_{xy}^1, d_{xz}^1, d_{yz}^1, d_{z^2}^1, d_{x^2-y^2}^0$ configuration (DOS not shown) and, hence, several $180^\circ \text{Mn}^{3+}\text{-O-Li}$ spin transfer mechanisms need to be considered (Table IV): a delocalization mechanism via the oxygen ion involving the d_{z^2} orbital in the (xy) plane (as described for $\text{La}_4\text{LiNiO}_8$), leading to a positive spin on Li and a polarization of the bonding $d_{x^2-y^2}\text{-}p_\sigma$ orbital by the unpaired spins in the d_{xy} , d_{yz} , d_{xz} , and d_{z^2} orbitals, leading to a negative spin on the O p_σ and Li $2s$ orbitals.

The electron spin difference in the xy plane [Fig. 6(b)] is similar to that obtained for $\text{La}_4\text{LiCrO}_8$ and a negative spin density is seen on the lithium site (Fig. 3). Therefore the polarization of the $d_{x^2-y^2}$ orbitals represents the predominant effect. While the polarization effect is the smaller of the two interactions in $\text{La}_4\text{LiNiO}_8$, it predominates in $\text{La}_4\text{LiMnO}_8$, consistent with the larger total moment on the Mn^{3+} ions.

The $\text{LiM}_y\text{Co}_{1-y}\text{O}_2$ phases ($M=\text{Cr}, \text{Ni}$). In the $\text{LiM}_y\text{Co}_{1-y}\text{O}_2$ phases ($M=\text{Cr}, \text{Ni}$), Li interacts with M^{3+} with either a 90° or $180^\circ M\text{-O-Li}$ angle. The spin polarization (up minus down spin) in a (M, O, Li) plane of the structure is plotted in order to visualize both types of interaction (Fig. 9). The positions of the different ions are also indicated. Table V summarizes the spin transfer mechanisms that occur in $\text{LiCr}_{1/8}\text{Co}_{7/8}\text{O}_2$ and $\text{LiNi}_{1/8}\text{Co}_{7/8}\text{O}_2$.

In $\text{LiCr}_{1/8}\text{Co}_{7/8}\text{O}_2$, the unpaired electrons are located in the t_{2g} orbitals of Cr^{3+} . Therefore, the following transfer mechanisms can take place, depending on the geometry of the interaction (Table V).

90° interaction: the hybridization of the $\text{Cr}^{3+} t_{2g}$, O p_π , and Li(3) $2s$ orbitals leads to a positive transferred spin density on Li by the delocalization mechanism. The calculated spin density is shown in Fig. 5(a).

180° interaction: the polarization of the bonding $e_g\text{-}p_\sigma\text{-}s$ orbital leads to a negative spin on the O p_σ orbital that points towards M and Li(2), as already discussed in the case of $\text{La}_4\text{LiCrO}_8$. The resulting spin transfer on Li(2) is therefore negative [Fig. 5(b)]. As a result, a positive NMR shift is predicted for Li(3) (90° interaction) and a negative one is predicted for Li(2) (180° interaction) in good agreement with the previous signal assignments [Figs. 9(a) and 3].¹⁰

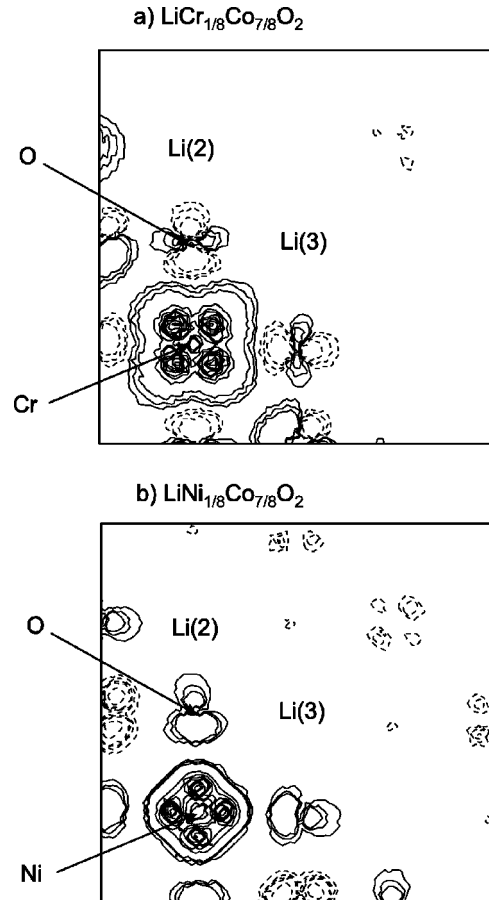


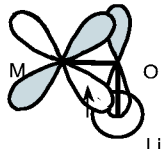
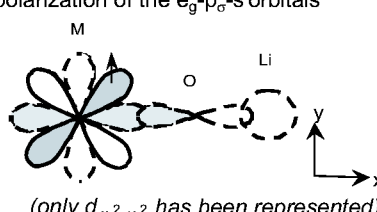
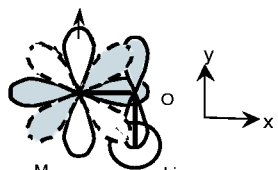
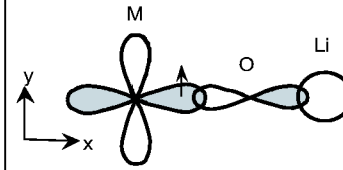
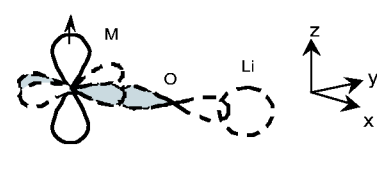
FIG. 9. Calculated spin polarization density map in a $M\text{-O-Li}$ plane in $\text{LiM}_{1/8}\text{Co}_{7/8}\text{O}_2$ with $M=\text{Cr}$ (a) and $M=\text{Ni}$ (b) from DFT calculations: solid line and dashed contours indicate positive and negative spin densities, respectively. Different contour steps were taken around O and M since the spin difference is much larger on M . The position of each ion is also indicated. The Li(2) and Li(3) are the notations also used in Fig. 1 and Table III: Li(1) has a M^{3+} ion as its second cation coordination shell and Li(2) has a M^{3+} ion in its first cation coordination shell.

The NiO_6 octahedra in $\text{LiNi}_{1/8}\text{Co}_{7/8}\text{O}_2$ are not Jahn-Teller distorted, as shown in the DOS for Ni (Fig. 10) (see also the $d_{\text{Ni-O}}$ bondlengths in Table II). Therefore, the two $\text{Ni}^{3+} e_g$ orbitals are almost degenerate and are both involved in the transfer mechanism. The following transfer mechanisms can occur (Table V).

90° interaction: the polarization by the e_g electron spin, of the doubly occupied $t_{2g}\text{-}p_\pi\text{-}s$ orbitals resulting from the hybridization of the $\text{Ni}^{3+} t_{2g}$, O p_π , and Li(3) $2s$ orbitals, leads to a negative spin on Li(3). Note that another polarization effect can occur on O ($e_g\text{-}p_\sigma\text{-}p_\pi\text{-}s$ overlap), leading to a negative spin on Li, but as it requires two O $2p$ orbitals it is weaker than the first one described above.

180° interaction: (a) the delocalization mechanism involving the singly occupied orbital results in a positive spin on the O p_σ orbital that points towards Ni and Li(2). (b) The spin in the partially occupied e_g orbital polarizes the bonding $e_g\text{-}p_\sigma\text{-}s$ orbital involving the second e_g orbital, leading to a negative spin on Li.

TABLE V. Illustration of the different mechanisms that result in transfer of spin density from a transition metal ion M to Li in the layered $\text{LiM}_{1/8}\text{Co}_{7/8}\text{O}_2$ ($M = \text{Cr}, \text{Ni}$) materials for two different $M\text{-O-Li}$ angles.

M in $\text{LiM}_{1/8}\text{Co}_{7/8}\text{O}_2$	involved spin orbital	M-O-Li angle	M-O-Li transfer	resulting sign on Li
Cr^{3+} (t_{2g}^3)	t_{2g}	90°	delocalization ($t_{2g}\text{-p}_\pi\text{-s}$ hybridization) 	positive
	t_{2g}	180°	polarization of the $e_g\text{-p}_\sigma\text{-s}$ orbitals  (only $d_{x^2-y^2}$ has been represented)	negative
Ni^{3+} ($t_{2g}^6 e_g^1$)	e_g	90°	polarization of the $t_{2g}\text{-p}_\pi\text{-s}$ orbitals  (only $d_{x^2-y^2}$ and d_{xy} are shown)	negative
		180°	delocalization ($e_g^*\text{-p}_\sigma\text{-s}$ hybridization)  (only $d_{x^2-y^2}$ is shown)	positive
	e_g	180°	polarization of the $e_g\text{-p}_\sigma\text{-s}$ orbitals  (only the polarization of $d_{x^2-y^2}\text{-p}_\sigma\text{-s}$ by the d_{z^2} unpaired electron is shown)	negative

Note that interactions directly involving only one of the two e_g orbitals (the $d_{x^2-y^2}$ orbital) are shown Table V. As seen in Figs. 9(b) and 3, the resulting spin density on the lithium ions is positive for Li(2) and negative for Li(3).

Therefore, the delocalization mechanism dominates for the 180° $M\text{-O-Li}$ interaction. As the same mechanism occurs in $\text{La}_4\text{LiNiO}_8$, the sign of the transferred spin density for a 180° interaction does not depend on whether the degeneracy

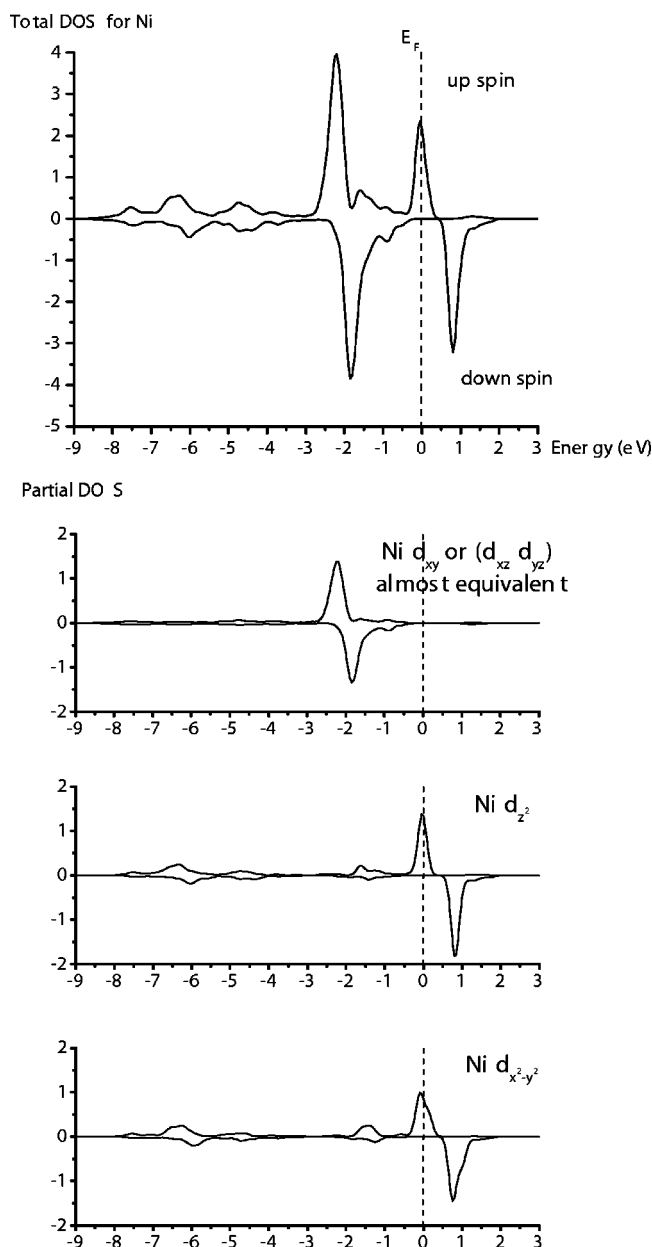


FIG. 10. The calculated total and partial density of state on Ni in $\text{LiNi}_{1/8}\text{Co}_{7/8}\text{O}_2$.

of the e_g orbitals has been lifted by the distortion of the NiO_6 octahedra. However, the spin density transferred to the lithium site for $\text{La}_4\text{LiNiO}_8$ is approximately four times smaller than that transferred to the lithium site in $\text{LiNi}_{1/8}\text{Co}_{7/8}\text{O}_2$ (Fig. 4), since there are four 180° M -O-Li interactions in $\text{La}_4\text{LiNiO}_8$ and only one in $\text{LiNi}_{1/8}\text{Co}_{7/8}\text{O}_2$. This is explained by the weaker overlap of the O p_σ orbitals with the lobe of the d_{z^2} orbital in the (xy) plane than with the lobes of the $d_{x^2-y^2}$ or d_{z^2} orbital that point directly towards the O p_σ orbital.

Overall, in the $\text{LiNi}_y\text{Co}_{1-y}\text{O}_2$ compounds, a negative NMR shift is predicted for Li(3) (a 90° interaction) and a positive one is predicted for Li(2) (a 180° interaction), in disagreement with the previous assignment of the +110 and -15 ppm signals, based on the transposition of the Good-

enough and Kanamori rules to the M -O-Li interaction.^{1,6} In this previous assignment,⁶ the polarization mechanism was neglected as it was assumed to be weak in comparison to the delocalization and to the correlation mechanisms, as it is usually considered in the case of interactions between two transition metal ions.⁵⁸ However, it is clear from our calculations that the main mechanism, in addition to delocalization, is the polarization of doubly occupied orbitals by the electron spins occupying higher energy orbitals.

The LiMO_2 phases ($M = \text{Cr}, \text{Mn}, \text{Fe}, \text{Ni}$). In the LiMO_2 phase, the spin transferred to Li results from its interaction with six M^{3+} as first neighbors and six M^{3+} as second neighbors. The spin density values calculated for the LiCrO_2 and LiNiO_2 materials are very close to the ones predicted by taking the individual contributions for the 90° and 180° interactions previously calculated for the $\text{LiM}_{1/8}\text{Co}_{7/8}\text{O}_2$ phases. The small differences can be ascribed to small changes in the cell parameters. We were not able to compute the single contributions of the 90° and 180° interactions for Fe-O-Li and Mn-O-Li as Fe^{3+} and Mn^{3+} ions were predicted to be low-spin in $\text{LiM}_{1/8}\text{Co}_{7/8}\text{O}_2$, whereas they adopt a high spin state in LiMO_2 . For occupation of both the t_{2g} and e_g orbitals, as occurs in Mn^{3+} and Fe^{3+} , the size and sign of the shift is not easily predicted as the delocalization and the polarization mechanisms lead to different signs for transfer involving the t_{2g} and e_g unpaired electrons.

The general trend of the predicted shifts is in good agreement with the experimental results for the LiMO_2 phases except for LiCrO_2 (Fig. 4), where a small, positive shift is seen experimentally. The positive shift for LiCrO_2 must be a result of the delicate balance between the two competing positive and negative shift mechanisms (i.e., the 90° and 180° interactions). However, the predicted shift (-210 ppm) for LiCrO_2 , estimated using the experimental values observed for single Li-O-Cr 90° and 180° interactions ($6 \times 35 \text{ ppm} + 6 \times -70 \text{ ppm}$ ¹⁰) in the magnetically dilute sample $\text{LiCr}_x\text{Co}_{1-x}\text{O}_2$ is consistent with the result for LiCrO_2 obtained from our calculations. This suggests that the increased magnetic couplings between the Cr^{3+} ions in LiCrO_2 may also change the sizes of the relative contributions of the two mechanisms.

As we noted earlier, the Jahn-Teller distortion of the MO_6 octahedra reduces the spin transferred in LiMnO_2 and LiNiO_2 [Fig. 4(b)]. Considering that the e_g orbitals are the most affected ones by the Jahn-Teller distortion, the 180° interaction must be the most modified, as the 90° interaction only involves the t_{2g} orbitals. We therefore discuss the shift decrease from the rhombohedral to the monoclinic cell considering only the 180° interactions. In the rhombohedral structure, both d_{z^2} and $d_{x^2-y^2}$ orbitals are involved in this transfer, as seen for $\text{LiNi}_{1/8}\text{Co}_{7/8}\text{O}_2$. In the monoclinic structure, only the d_{z^2} - p - s transfer will be weakened due to an increase in the M -O bond in the z direction, whereas the interactions in the (xy) plane should be strongest because of the shorter M -O-Li distances. We saw for La_4LiMO_8 and $\text{LiNi}_{1/8}\text{Co}_{7/8}\text{O}_2$ that these 180° in (xy) -plane interactions were associated with either a negative spin transfer or a weak positive one. As a result, the spin transferred on Li and thus

the shift predicted for the monoclinic LiMO_2 ($M = \text{Ni}, \text{Mn}$) will be weaker than that predicted for rhombohedral LiMO_2 (no Jahn-Teller distorted MO_6).

C. Effect of the temperature on the shifts

Because $\langle S_z \rangle$ in Eq. (1) is proportional to $B_0\chi$ as given in Eq. (2), the Fermi contact interaction should show the same temperature behavior as the magnetic susceptibility. A compound exhibiting Curie Weiss susceptibility will therefore exhibit a lithium shift that is inversely proportional to temperature. The temperature dependent NMR spectroscopy can thus identify magnetic phase transitions in a solid: Lee *et al.* used ^6Li MAS NMR to demonstrate that in orthorhombic LiMnO_2 a magnetic phase transition from short-range spin ordering to a long-range antiferromagnetic ordering occurs as temperature decreases.⁴⁷

In our calculations, the spin density around the lithium ions are calculated at 0 K in a situation where all the electron spins are aligned with the applied magnetic field (i.e., the magnetization is saturated). In such a case, the susceptibility is not defined. Referring to Eq. (1), we can nevertheless scale the calculated Fermi contact shift with the one expected at room temperature (RT), provided the RT susceptibility is known.

We can rewrite the contact shift, expressed in Hz, for a given applied magnetic field as

$$\Delta\omega = -\frac{A_c}{\hbar}\langle S_z \rangle = \frac{A_c}{\hbar}\mu_0 g N_0 \mu_B \chi_M B_0. \quad (4)$$

Therefore, the shift in Hertz is proportional to the magnetization $B_0\chi$. At 0 K, whatever the field, the magnetization value is the saturation one, i.e., $2S\mu_B$, S being the total spin per mole of the material, which can be calculated provided the electronic configuration of the transition elements is known. At any temperature and any field in the regime corresponding to the NMR experiment, the magnetization is given by $B_0\chi$, and can either be calculated provided the magnetic behavior is known (Curie or Curie-Weiss law), or measured experimentally. Therefore, the scaling factor required to calculate a RT contact shift (in Hertz, and therefore also in ppm) using our calculated spin densities is, in principle, known for a given compound.

The relative magnitudes of the contact shift as shown in Fig. 4 do not necessarily reflect the expected relative magnitudes at room temperature as the different compounds exhibit

different magnetic behaviors. Lee *et al.* suggested that the presence of short-range $\text{Mn}^{3+}\text{-Mn}^{3+}$ antiferromagnetic couplings that persist at ambient temperatures for this compound, contributes to the small value of the shift observed experimentally for LiMnO_2 and is the cause for its weak temperature dependence.⁴⁷ That is the presence of adjacent Mn^{3+} ions with opposite spin results in the transfer of spin density with opposite polarity to the lithium ion serving to reduce the Li hyperfine shift. Therefore the resulting spin density at RT on Li should be smaller than that in hypothetical paramagnetic (Curie-like) LiMnO_2 . Finally, the small shift observed experimentally for LiMnO_2 must be due to the sum of two effects: AF Mn-Mn short-range coupling and Jahn-Teller distortion of the MnO_6 octahedra.

VI. CONCLUSIONS

We show that density functional theory calculations are a useful tool to interpret the observed paramagnetic shifts in layered oxides and allow us to elucidate the major transfer processes, i.e., delocalization and polarization mechanisms. This information can be used to predict the magnitudes and signs of the Li hyperfine shifts in other compounds with different Li local environments and electronic configuration of the transition metal ion. Especially, such calculations can be used to predict shifts in structures where the Li- M -O angle is different from 90° or 180° . Furthermore, a precise experimental knowledge of the magnetic susceptibility of any compound should allow us to estimate that actual value of the contact shift at the temperature corresponding to the NMR measurement.

We believe that such calculations can become an important tool to identify NMR paramagnetic shifts and hence further enhance the applicability of NMR as a detailed local probe. NMR spectroscopy also serves as an important method for testing predictions based on first-principles calculations.

ACKNOWLEDGMENTS

The authors wish to thank Dane Morgan for fruitful discussions and the French ministry of foreign affairs and the NSF/CNRS exchange grants (Grant No. NSF-INT-0003799) for financial support. The Center for Materials Science and Engineering and the Singapore-MIT Alliance are also gratefully thanked for financial support. C.P. Gray thanks the NSF (Grant Nos. DMR 9901308 and 0211353) for support.

*Electronic address: dany_carlier@yahoo.com

¹C. Marichal, J. Hirschinger, P. Granger, M. Ménétrier, A. Rougier, and C. Delmas, *Inorg. Chem.* **34**, 1773 (1995).

²R. Alcantara, P. Lavela, P. L. Relano, J. L. Tirado, E. Zhecheva, and R. Stoyanova, *Inorg. Chem.* **37**, 264 (1998).

³I. Tomeno and M. Oguchi, *J. Phys. Soc. Jpn.* **67**, 318 (1998).

⁴M. P. J. Peeters, M. J. Van Bommel, P. M. C. Neilen-tenWolde, H. A. M. Van Hal, W. C. Keur, and A. P. M. Kentgens, *Solid State Ionics* **112**, 41 (1998).

⁵S. Levasseur, M. Ménétrier, E. Suard, and C. Delmas, *Solid State Ionics* **128**, 11 (2000).

⁶D. Carlier, M. Ménétrier, and C. Delmas, *J. Mater. Chem.* **11**, 594 (2001).

⁷E. Gaudin, F. Taulelle, R. Stoyanova, E. Zhecheva, R. Alcantara, P. Lavela, and J. L. Tirado, *J. Phys. Chem. B* **105**, 8081 (2001).

⁸Y. J. Lee, S.-H. Park, C. Eng, J. B. Parise, and C. P. Grey, *Chem. Mater.* **14**, 194 (2002).

⁹Y. J. Lee and C. P. Grey, *J. Phys. Chem. B* **106**, 3576 (2002).

- ¹⁰C. Pan, Y. J. Lee, B. Amundsen, and C. P. Grey, *Chem. Mater.* **14**, 2289 (2002).
- ¹¹G. Maruta, S. Takeda, R. Imachi, T. Ishida, T. Nogami, and K. Yamaguchi, *J. Am. Chem. Soc.* **121**, 424 (1999).
- ¹²H. Heise, F. H. Köhler, F. Mota, J. J. Novoa, and J. Veciana, *J. Am. Chem. Soc.* **121**, 9659 (1999).
- ¹³C. Kohler, G. Seifert, U. Gerstmann, M. Elstner, H. Overhof, and T. Frauenheim, *Phys. Chem. Chem. Phys.* **3**, 5109 (2001).
- ¹⁴F. H. Köhler, *Magnetism: Molecules to Materials* (Wiley-VCH, New York, 2001).
- ¹⁵L. B. Knight, J. G. Kaup, B. Petzoldt, R. Ayyad, T. Ghanty, and R. Davidson, *J. Chem. Phys.* **110**, 5658 (1999).
- ¹⁶C. Delmas and I. Saadoune, *Solid State Ionics* **53-56**, 370 (1992).
- ¹⁷C. Delmas, I. Saadoune, and A. Rougier, *J. Power Sources* **43-44**, 595 (1993).
- ¹⁸A. Ueda and T. Ohzuku, *J. Electrochem. Soc.* **141**, 2010 (1994).
- ¹⁹R. Alcantara, J. Morales, J. L. Tirado, R. Stoyanova, and E. Zhecheva, *J. Electrochem. Soc.* **142**, 3997 (1995).
- ²⁰I. Saadoune and C. Delmas, *J. Mater. Chem.* **6**, 193 (1996).
- ²¹D. Caurant, N. Baffier, B. Garcia, and J. P. Pereira-Ramos, *Solid State Ionics* **91**, 45 (1996).
- ²²W. Li and C. Currie, *J. Electrochem. Soc.* **14**, 2773 (1997).
- ²³R. Alcantara, P. Lavela, J. L. Tirado, R. Stoyanova, and E. Zhecheva, *J. Electrochem. Soc.* **145**, 730 (1998).
- ²⁴J. Cho, G. Kim, and H. S. Lim, *J. Electrochem. Soc.* **146**, 3571 (1999).
- ²⁵K. Numata, C. Sakaki, and S. Yamanaka, *Chem. Lett.* **8**, 725 (1997).
- ²⁶K. Numata, C. Sakaki, and S. Yamanaka, *Solid State Ionics* **117**, 257 (1999).
- ²⁷K. Numata and S. Yamanaka, *Solid State Ionics* **118**, 117 (1999).
- ²⁸B. Amundsen, J. M. Paulsen, I. Davidson, R. S. Liu, C. H. Shen, J. M. Chen, L. Y. Jang, and J. F. Lee, *J. Electrochem. Soc.* **149**, A431 (2002).
- ²⁹Z. Lu, D. D. MacNeil, and J. R. Dahn, *Electrochem. Solid-State Lett.* **4**, A191 (2001).
- ³⁰Z. Lu, L. Y. Beaulieu, R. A. Donabarger, C. L. Thomas, and J. R. Dahn, *J. Electrochem. Soc.* **149**, A778 (2002).
- ³¹Z. Lu and J. R. Dahn, *J. Electrochem. Soc.* **149**, A815 (2002).
- ³²C. Delmas, C. Fouassier, and P. Hagenmuller, *Physica B* **99**, 81 (1980).
- ³³T. A. Hewston and B. L. Chamberland, *J. Phys. Chem. Solids* **48**, 97 (1987).
- ³⁴Y. I. Jang, F. C. Chou, and Y. M. Chiang, *J. Phys. Chem. Solids* **60**, 1763 (1999).
- ³⁵M. Tabuchi, K. Ado, H. Kobayashi, I. Matsubara, H. Kageyama, M. Wakita, S. Tsutsui, S. Nasu, Y. Takeda, C. Masquelier, A. Hirano, and R. Kanno, *J. Solid State Chem.* **141**, 554 (1998).
- ³⁶A. R. Armstrong and P. G. Bruce, *Nature (London)* **381**, 499 (1996).
- ³⁷F. Capitaine, P. Gravereau, and C. Delmas, *Solid State Ionics* **89**, 197 (1996).
- ³⁸A. Rougier, C. Delmas, and A. V. Chadwick, *Solid State Commun.* **94**, 123 (1995).
- ³⁹S. Abou-Warda, W. Pietzuch, G. Berghoefer, U. Kesper, W. Massa, and D. Reinen, *J. Solid State Chem.* **138**, 18 (1998).
- ⁴⁰G. Demazeau, E. O. Okhim, K. T. Wang, L. Fourmes, J. M. Dance, M. Pouchard, and P. Hagenmuller, *Rev. Chim. Miner.* **24**, 183 (1987).
- ⁴¹J. C. Burley, D. Battle, D. J. Gallon, J. Sloan, C. P. Grey, and M. J. Rosseinsky, *J. Am. Chem. Soc.* **124**, 620 (2002).
- ⁴²H. M. McConnell and R. E. Robertson, *J. Chem. Phys.* **29**, 1361 (1958).
- ⁴³H. M. McConnell and D. B. Chesnut, *J. Chem. Phys.* **28**, 107 (1958).
- ⁴⁴C. Kittel, *Introduction to Solid State Physics* (Wiley, New York, 1986).
- ⁴⁵G. Kresse and J. Furthmuller, *Comput. Mater. Sci.* **6**, 15 (1996).
- ⁴⁶R. D. Shannon and C. T. Prewitt, *Acta Crystallogr., Sect. B: Struct. Crystallogr. Cryst. Chem.* **25**, 925 (1969).
- ⁴⁷Y. J. Lee and C. P. Grey, *Chem. Mater.* **12**, 3871 (2000).
- ⁴⁸B. Ouyang, X. Cao, H. W. Lin, S. Slane, S. Kostov, M. d. Boer, and S. G. Greenbaum, in *Solid-State Ionics IV*, edited by G.-A. Nazri *et al.*, Mater. Res. Soc. Symp. Proc. No. 369 (Materials Research Society, Pittsburgh, 1995), p. 59.
- ⁴⁹M. Carewska, S. Scaccia, S. Arumugam, Y. Wang, and S. Greenbaum, *Solid State Ionics* **93**, 227 (1997).
- ⁵⁰T. J. Boyle, D. Ingersoll, T. M. Alam, C. J. Tafoya, M. A. Rodriguez, K. Vanheusden, and D. H. Dougherty, *Chem. Mater.* **10**, 2270 (1998).
- ⁵¹R. Alcantara, P. Lavela, J. L. Tirado, E. Zhecheva, and R. Stoyanova, *J. Electroanal. Chem.* **454**, 173 (1998).
- ⁵²N. Imanishi, M. Fujiyoshi, Y. Takeda, O. Yamamoto, and M. Tabuchi, *Solid State Ionics* **118(1-2)**, 121 (1999).
- ⁵³M. Ménétrier, I. Saadoune, S. Levasseur, and C. Delmas, *J. Mater. Chem.* **9**, 1135 (1999).
- ⁵⁴D. Carlier, Ph.D. thesis, University of Bordeaux I, 2001.
- ⁵⁵P. Ganguly, T. N. Venkatraman, S. Pradhan, P. R. Rajamohanan, and S. Ganapathy, *J. Phys. Chem.* **100**, 5017 (1996).
- ⁵⁶S. K. Mishra and G. Ceder, *Phys. Rev. B* **59**, 6120 (1999).
- ⁵⁷C. A. Marianetti, D. Morgan, and G. Ceder, *Phys. Rev. B* **63**, 224 304 (2001).
- ⁵⁸J. B. Goodenough, *Magnetism and the Chemical Bonds* (Wiley, New-York, 1963).